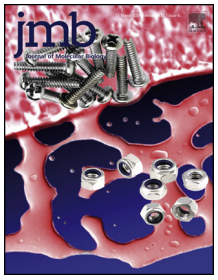

Conformational Dynamics of Damage Processing by Human DNA Glycosylase NEIL1

Olga A. Kladova†, Inga R. Grin†, Olga S. Fedorova, Nikita A. Kuznetsov and Dmitry O. Zharkov

SB RAS Institute of Chemical Biology and Fundamental Medicine, *8 Lavrentieva Ave., Novosibirsk 630090, Russia*
Novosibirsk State University, *2 Pirogova St., Novosibirsk 630090, Russia*

Correspondence to Nikita A. Kuznetsov and Dmitry O. Zharkov: *SB RAS Institute of Chemical Biology and Fundamental Medicine, 8 Lavrentieva Ave., Novosibirsk 630090, Russia. kladova@niboch.nsc.ru, grin@niboch.nsc.ru, fedorova@niboch.nsc.ru, nikita.kuznetsov@niboch.nsc.ru, dzharkov@niboch.nsc.ru*
https://doi.org/10.1016/j.jmb.2019.01.030
Edited by M Gottesman

Abstract

Endonuclease VIII-like protein 1 (NEIL1) is a DNA repair enzyme found in higher eukaryotes, including humans. It belongs to the helix–two turn–helix (H2TH) structural superfamily together with *Escherichia coli* formamidopyrimidine–DNA glycosylase (Fpg) and endonuclease VIII (Nei), and removes a variety of oxidized purine and pyrimidine bases from DNA. Structural, modeling and kinetic studies have established that the bacterial H2TH superfamily enzymes proceed through several conformational intermediates while recognizing and removing their cognate lesions. Here we apply stopped-flow kinetics with detection of intrinsic Trp fluorescence and Förster resonance energy transfer fluorescence to follow the conformational dynamics of human NEIL1 and DNA when the enzyme interacts with undamaged DNA, or DNA containing cleavable or non-cleavable abasic sites, or dihydrouracil lesions. NEIL1 processed a natural abasic site and a damaged base in DNA equally well but showed an additional fluorescently discernible step when DHU was present, likely reflecting additional rearrangements during base eversion into the enzyme's active site. With undamaged DNA and DNA containing a non-cleavable abasic site analog, (3-hydroxytetrahydrofuran-2-yl) methyl phosphate, NEIL1 was diverted to a non-productive DNA conformation early in the reaction. Our results support the view of NEIL1 as an enzyme that actively destabilizes damaged DNA and uses multiple checkpoints along the reaction coordinate to drive substrate lesions into the active site while rejecting normal bases and non-substrate lesions.

Introduction

Reactive oxygen species appear in cells as byproducts of aerobic respiration and may be also generated by environmental sources such as various chemicals, UV and ionizing radiation [1,2]. They react with DNA to produce a variety of genotoxic lesions that contribute to aging and a number of diseases [2–4]. Oxidized DNA moieties are recognized and removed by the base excision repair (BER) system, which includes lesion-specific DNA glycosylases, apurinic/apyrimidinic (AP) endonucleases, DNA polymerases and DNA ligases [5,6].

DNA glycosylases are responsible for finding chemically modified bases and catalyzing their excision from DNA. Two *Escherichia coli* DNA glycosylases belonging to the helix–two-turn–helix (H2TH) superfamily, formamidopyrimidine–DNA glycosylase (Fpg) and endonuclease VIII (Nei), remove oxidized purines and pyrimidines, respectively [7,8]. In human cells, three Nei-like proteins, NEIL1, NEIL2, and NEIL3, have been characterized [8,9]. NEIL1 has broad substrate specificity, removing both pyrimidine- and purine-derived lesions from DNA [10–15]. NEIL2 activity primarily excises oxidative derivatives of cytosine and has preference for the lesion in bubbles resembling transcription intermediates [16–18]. NEIL3 mainly removes advanced products of purine oxidation from single-stranded DNA and has a very restricted tissue distribution

suggestive of a role in development or cell regulation [19,20].

Members of the H2TH superfamily are bifunctional enzymes capable of catalyzing hydrolysis of the *N*-glycosidic bond followed by β,δ-elimination, thus introducing a single-nucleoside gap into DNA [7,21]. They all use an N-terminal amino group (Val1 in NEIL3, Pro1 in all other homologs) to attack at C1′ of the damaged nucleotide and form a Schiff base-type covalent reaction intermediate [16,22–24].

Several three-dimensional structures of Fpg, Nei, and NEILs as well as their complexes with DNA have been determined [25–38]. The recognition of the substrate lesions by these enzymes involves extensive conformational changes in both protein and DNA, such as closing of the protein domains, DNA kinking, damaged base eversion out of the DNA helix into the enzyme's active site and intrusion of several amino acid side chains into DNA. In particular, H2TH proteins diverge in two important structural elements: the residues that are inserted into the void created in DNA by the eversion of the damaged nucleotide, and the "missing loop" that forms the base-recognition pocket and is disordered in all DNA-bound structures lacking the cognate base.

Previously, we had applied stopped-flow kinetics with fluorescence detection to analyze the dynamics of conformational transitions during substrate binding and cleavage by two members of the H2TH superfamily, *E. coli* Fpg and Nei [39–48]. Based on several detectable sequential changes in the Trp fluorescence of Fpg, using a series of DNA substrates of different structure, and supplementing this with other reporters (2-aminopurine, pyrrolocytosine, 1,3-diaza-2-oxophenoxazine, 3-hydroxychromone) strategically incorporated at different places in DNA, we have been able to single out and attribute five reversible steps in the lesion recognition followed by an irreversible step, presumably corresponding to the reaction chemistry, and then the product release step (Scheme 1). In Fpg, the sequential reversible steps in Scheme 1 correspond to the following: (i) non-specific primary encounter, (ii) initial recognition with the destabilization of the DNA around the lesion with the insertion of Phe110, (iii) kinking the DNA axis, (iv) eversion of oxoG base from the double helix into the enzyme's active site and filling the resulting void in the double helix by Arg-108 and Met-73, and (v) isomerization of the enzyme to a catalytically competent conformation. With Nei, only three reversible steps were observed by Trp fluorescence before the irreversible one, and the second of them corresponded to two DNA conformational changes revealed by 3-hydroxychromone reporter fluorescence. The similarity of Fpg and Nei structures suggests that their substrate recognition mechanisms should be similar, yet some of the steps may remain not discernible if Trp residues are located unfavorably in the protein structure.

In the present work, we apply the same strategy to improve the current understanding of damage recognition by human NEIL1. We have used a series of duplexes that contain guanine, (3-hydroxytetrahydrofuran-2-yl)methyl phosphate (F), AP site, or 5,6-dihydrouracil (DHU), henceforth referred to as G-ligand, F-ligand, AP-substrate, and DHU-substrate, respectively. Conformational changes in the protein were monitored by changes in Trp fluorescence intensity. Förster resonance energy transfer (FRET) measurements were used for analysis of conformational changes of model DNA substrates modified at 5′ termini with the dye–quencher pair FAM/BHQ1. Drawing upon our data and available structural information for H2TH superfamily enzymes, we propose the most likely sequence of events leading to the formation of the catalytically active complex in NEIL1.

Results

Rationale and experiment design

Stopped-flow studies of several bifunctional DNA glycosylases, including bacterial members of the H2TH superfamily, revealed that the recognition involves non-specific DNA binding followed by several conformational rearrangements of the enzyme–DNA complex if a cognate DNA substrate is present (reviewed in Refs. [43,49]). Non-specific binding in these enzymes usually can be minimally described by a two-state equilibrium and is characterized by similar rate constants for both damaged and undamaged DNA. DNA containing F, an uncleavable analog of a cognate abasic lesion, can then enter productive reaction path, which ends in a dead-end complex. An aldehydic AP site follows the same conformational path as F but the reaction proceeds to forming the β-elimination product, allowing the catalytic rate constant of the AP lyase reaction to be estimated. Finally, if the cognate damaged base is present, an extra equilibrium step is usually observed, reflecting the adjustment of base-binding pocket as a final recognition step, and the cleavage sometimes may be kinetically separated into base excision and β-elimination phases. Therefore, the minimal substrate

$$\mathrm{E{+}S} \overset{\text{(i)}}{\rightleftarrows} \mathrm{ES1} \overset{\text{(ii)}}{\rightleftarrows} \mathrm{ES2} \overset{\text{(iii)}}{\rightleftarrows} \mathrm{ES3} \overset{\text{(iv)}}{\rightleftarrows} \mathrm{ES4} \overset{\text{(v)}}{\rightleftarrows} \mathrm{ES5} \rightarrow (\mathrm{EP} \rightleftarrows \mathrm{E} + \mathrm{P})$$

Scheme 1. Recognition of oxoG-containing DNA by Fpg.

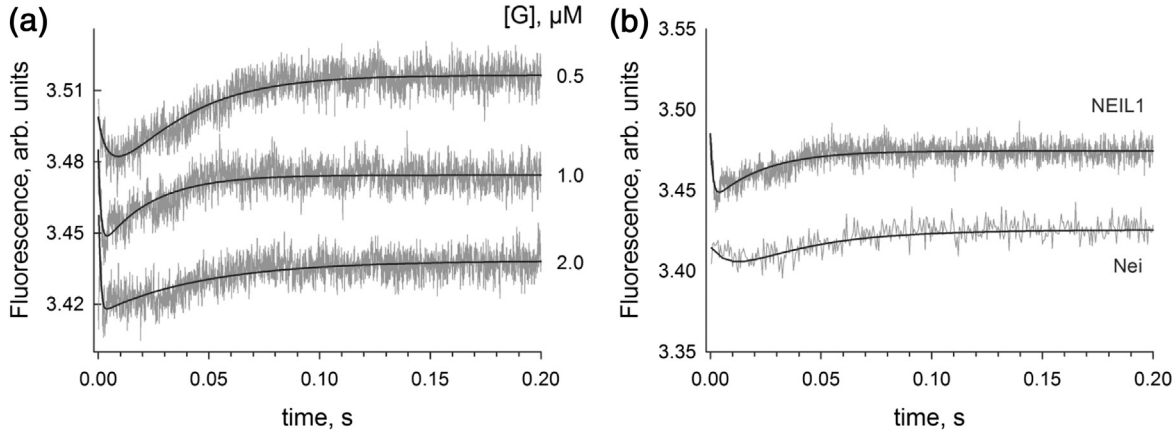

Fig. 1. Observed (jagged traces) and fitted (smooth curves) time courses of Trp fluorescence changes during non-specific G-ligand binding by NEIL1 (a). The concentration of NEIL1 was 1 μM. The concentration of G-ligand is shown to the right of the panel. The traces for NEIL1 and Nei obtained with 1 μM G-ligand under the identical conditions [45] are shown for comparison (b).

set producing useful kinetic schemes that can be dissected to reaction steps attributable to conformational changes in the glycosylase–DNA complex includes undamaged DNA and DNA containing F, AP, and a cognate damaged base [40,45,50,51]. Here, we have applied the same strategy for NEIL1. The length (12-mer) and basic sequence of the oligonucleotides in the stopped-flow Trp fluorescence experiments were the same as used before for Fpg and Nei to minimize the effects of non-target binding and to facilitate comparison with other H2TH superfamily enzymes.

NEIL1 conformational changes detected by Trp fluorescence

Non-specific DNA

After mixing nonspecific G-ligand with NEIL1, the binding was essentially complete by 0.1 s (Fig. 1a). The intensity of Trp fluorescence first quickly decreased and then gradually increased (Fig. 1a). The two-state equilibrium scheme produced a poor fit (not shown). Fitting the experimental data to the two-step binding model (Scheme 2) gave the values for the forward and reverse rate constants listed in Table 1. Kinetic curves in Fig. 1b show that the path to the encounter complex is likely similar for NEIL1 and Nei proteins. Although these two proteins cannot be directly compared with respect to the attribution of Trp fluorescent signal changes (see below), both NEIL1 and Nei may undergo similar conformational rearrangements in the course of non-specific DNA binding. It should be noted that the bimolecular encounter step for the eukaryotic protein was about an order of magnitude faster (Table 1 and data in [45]).

$$\mathrm{E} + \mathrm{L} \underset{k_{-1}}{\overset{k_1}{\rightleftarrows}} \mathrm{EL1} \underset{k_{-2}}{\overset{k_2}{\rightleftarrows}} \mathrm{EL2}$$

Scheme 2. Recognition of G- and F-ligands by NEIL1.

F-ligand

The fluorescence traces obtained for the uncleavable F-ligand are presented in Fig. 2. Binding of the F-ligand by NEIL1 led to a fast two-phase decrease in the Trp fluorescence intensity, and the fluorescence did not change after 0.1–0.2 s. Notably, during F-ligand binding, the intensity of Trp fluorescence first quickly decreased, as in the case of G-ligand, whereas the second phase was different for damaged and undamaged DNA, indicating that specific recognition of the F-site occurs at the second binding step. Similarly to the G-ligand binding, the traces could be fitted by a two-step equilibrium scheme (Scheme 2).

The rate constants of individual reaction steps (Table 1) extracted from fitting were of the same order of magnitude as in the case of the G-ligand. Therefore, the overall stability of NEIL1 complexes did not change much between normal and uncleavable abasic DNA, despite the apparently different conformational nature of G- and F-ligand binding.

Interestingly, the fluorescence traces observed for NEIL1 were different in their shapes from the traces obtained previously for Nei [45] and Fpg [40] (Fig. 2b). These enzyme-specific features of the specific recognition of F could stem both from Trp distribution in the proteins and from different interactions during the formation of the complex.

AP-substrate

If an aldehydic AP site is present in DNA, its recognition by NEIL1 is followed by sequential

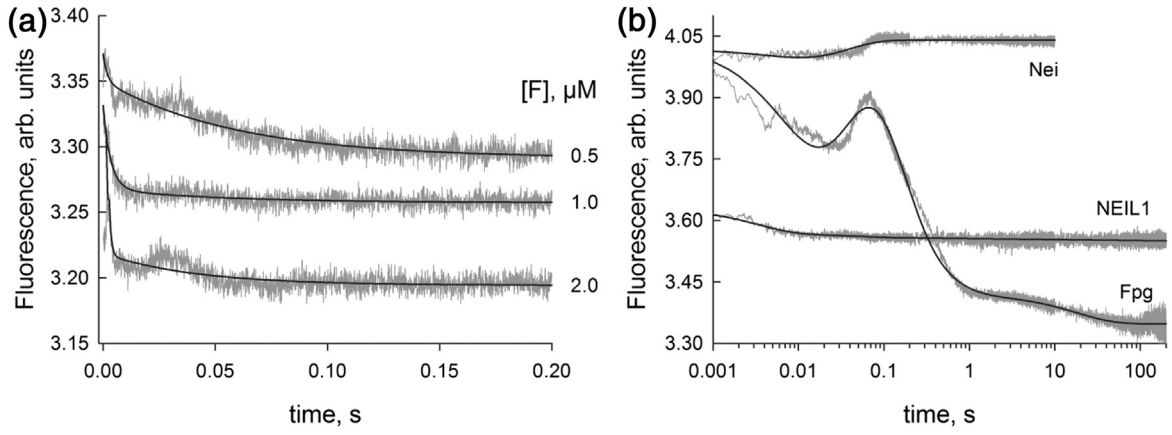

Fig. 2. Observed (jagged traces) and fitted (smooth curves) time courses of Trp fluorescence changes during F-ligand binding by NEIL1 (a). The concentration of NEIL1 was 1 μM. The concentration of F-ligand is shown to the right of the panel. The traces for NEIL1, Fpg and Nei obtained with 1 μM F-ligand under the identical conditions [40,45] are shown for comparison (b).

elimination of the 3′-phosphate (β-elimination) and 5′-phosphate (δ-elimination) and then dissociation of the enzyme–product complex. Conformational changes of NEIL1 in the course of binding the AP-substrate were characterized by more pronounced changes in Trp fluorescence intensity and the shape more complicated than in the case of non-cleavable ligands (Fig. 3a).

The transition from the uncleavable F-ligand to the cleavable AP-substrate did not change the fluorescence trends at the early reaction stages; the traces still decreased with time. All processes leading to a productive catalytic complex—encounter, wedging, eversion, void-filling and adjustment of protein and DNA conformations to achieve the catalytically competent state occurred within ~10 s (Fig. 3a). The traces had a pronounced wide minimum at ~5–20 s, which, in Fpg and Nei, corresponds to the irreversible catalytic step, and then increased and leveled off, reflecting the equilibrium between the enzyme–product complex and free enzyme and cleaved DNA. The minimal kinetic scheme (Scheme 3) describing the observed changes of Trp fluorescence intensity contained three equilibrium steps followed by an irreversible step and then an equilibrium step of product release (Table 1).

Comparing the elementary reaction rates for the F-ligand and the AP-substrate, NEIL1 showed a clear preference for the cleavable substrate: whereas the second equilibrium was shifted towards the EL1 intermediate (Scheme 2) for the F-ligand, the intermediates were efficiently partitioned forward for

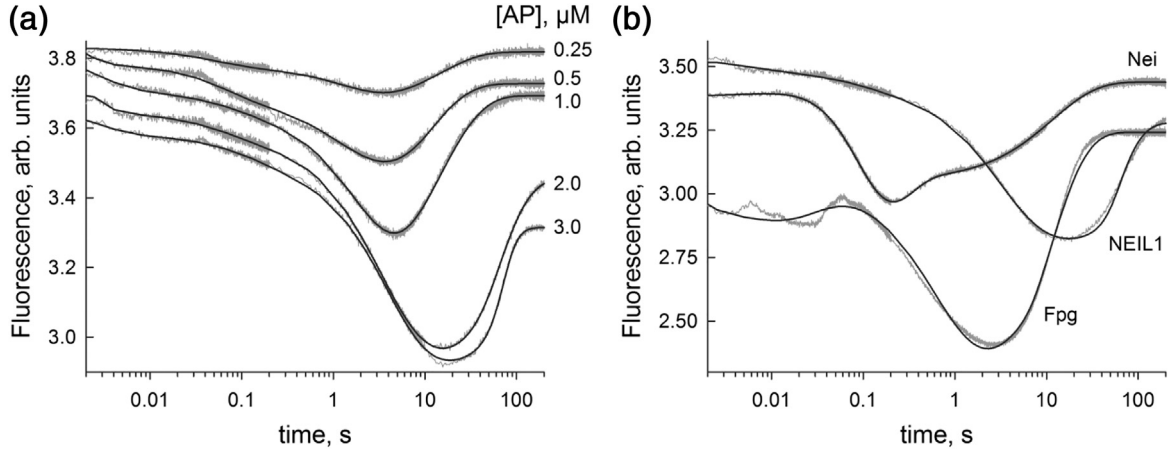

Fig. 3. Observed (jagged traces) and fitted (smooth curves) time courses of Trp fluorescence changes during AP-substrate binding and cleavage by NEIL1. The concentration of NEIL1 was 1 μM. The concentration of AP-substrate is shown to the right of the panel. The traces for NEIL1, Fpg and Nei obtained with 1 μM AP-substrate under the identical conditions [40,45] are shown for comparison (b).

$$E+S \underset{k_{-1}}{\overset{k_1}{\rightleftarrows}} ES1 \underset{k_{-2}}{\overset{k_2}{\rightleftarrows}} ES2 \underset{k_{-3}}{\overset{k_3}{\rightleftarrows}} ES3 \xrightarrow{k_4} \left(EP \overset{K_P}{\rightleftarrows} E + P \right)$$

Scheme 3. Recognition of AP-substrate by NEIL1.

the AP-substrate. Overall, the relative affinity (in terms of K_{bind}) of NEIL1 for the AP site was 200 times higher in comparison with the F-ligand.

The same kinetic mechanism (Scheme 3) was previously obtained for Nei [45], whereas the kinetic scheme for Fpg cleaving the AP site contained an additional reversible pre-catalytic step [40,41]. Nevertheless, as shown in Fig. 3b, the traces for NEIL1, Fpg and Nei obtained under the identical conditions are very different, indicating that conformational changes of enzymes detected by Trp fluorescence cannot be directly compared even for DNA glycosylases of the same structural superfamily. However, a common feature of all kinetic traces is a local minimum of Trp fluorescence intensity corresponding to the formation of the catalytic complex.

DHU-substrate

NEIL1 catalyzes hydrolysis of the *N*-glycosidic bond and β,δ-elimination of nucleotides containing damaged bases, in particular DHU [52]. The fluorescent traces characterizing the interaction of NEIL1 with the DHU-substrate had a shape similar to the traces for the AP-substrate (Fig. 4a). Nevertheless, an additional phase of the fluorescence changes could be fitted at the early part of the traces (~30 ms). Essentially, the step described by a pair of rate constants k_2 and k_{-2} for the AP-substrate was separated in two discernible steps with the DHU-substrate (Scheme 4). Notably, the equilibrium constants for the single step with the AP-substrate ($K = k_2/k_{-2}$) and the combined steps with the DHU-substrate ($K = (k_2/k_{-2})(1 + k_3/k_{-3})$) differed only ~2.1-fold (33.3 and 72.2, respectively; Table 1). The following reversible stage that immediately precedes the irreversible catalytic stage was also similar in terms of the equilibrium constant for the AP-substrate and DHU-substrate (14.7 and 24.5), although both forward and reverse rate constants were higher when the damaged base was present (Table 1). Finally, the irreversible catalytic step was also quite similar for both substrates (Table 1); as in the case of Fpg and Nei [40,41,45] and at variance with OGG1 [50,53], this step could not be separated into stages reflecting the base excision and the phosphate elimination.

DNA conformational changes detected by FRET

Dye-labeled duplexes were used for FRET analysis of DNA conformational changes during the interaction with NEIL1. As shown in Fig. 5a and b, binding of the FAM/BHQ-carrying C- and F-ligands by NEIL1 caused a slow decrease in the fluorescence intensity up to 500 s. This decrease reflects the FAM fluorophore and the BHQ1 quencher coming closer together when DNA bends in a complex with NEIL1. This similarity contrasts the differences in the fast conformational changes of enzyme molecule within 0.2 s detected by Trp fluorescence in the cases of undamaged duplex and F-containing DNA. The slow and similar FRET signal decreases indicate that DNA binding by NEIL1 kinks the DNA irrespectively of

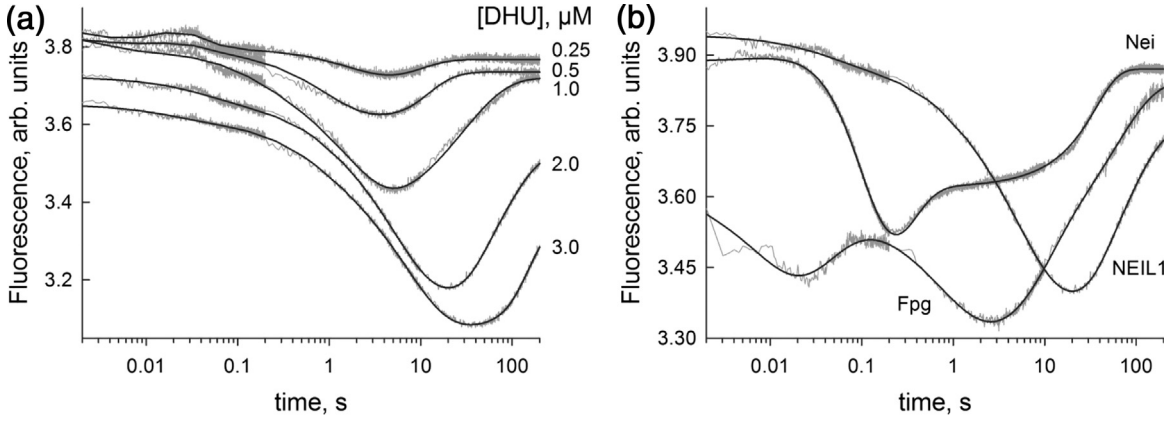

Fig. 4. Observed (jagged traces) and fitted (smooth curves) time courses of Trp fluorescence changes during DHU-substrate binding and cleavage by NEIL1 (a). The concentration of NEIL1 was 1 μM. The concentration of DHU-substrate is shown to the right of the panel. The traces for NEIL1, Fpg and Nei obtained with 1 μM DHU-substrate under the identical conditions [40,45] are shown for comparison (b).

$$\mathrm{E+S} \underset{k_{-1}}{\overset{k_1}{\rightleftarrows}} \mathrm{ES1} \underset{k_{-2}}{\overset{k_2}{\rightleftarrows}} \mathrm{ES2} \underset{k_{-3}}{\overset{k_3}{\rightleftarrows}} \mathrm{ES3} \underset{k_{-4}}{\overset{k_4}{\rightleftarrows}} \mathrm{ES4} \overset{k_5}{\rightarrow} \left(\mathrm{EP} \overset{K_\mathrm{P}}{\rightleftarrows} \mathrm{E+P} \right)$$

Scheme 4. Recognition of DHU-substrate by NEIL1.

whether it is damaged or not. The kinetic curves obtained for the FAM-C-BHQ- and FAM-F-BHQ-ligands could be fitted to a two-step mechanism (Scheme 2) to obtain rate and equilibrium constants (Table 2). The rate constants for primary complex formation EL1 had similar values, whereas the second binding step proceeded 7.5 times faster for the FAM-F-BHQ-ligand.

Interaction of NEIL1 with cleavable FAM-AP-BHQ- and FAM-DHU-BHQ-substrates includes formation of the pre-catalytic complex, catalytic reactions and dissociation of the enzyme–product complex. Binding of both substrates led to a decrease in the FRET signal up to 1 s; importantly, non-cleavable ligands showed much lower fluorescence change over this time. Cleavage and dissociation of the enzyme–product complex cause an increase in the FRET signal due to separation of FAM and BHQ1 labels.

The minimal kinetic Scheme 5 describes the observed FRET signal. The first and second steps reflect substrate binding and combined conformational changes on the way to the catalytically active complex ES2. The irreversible step corresponds to the catalytic reactions and dissociation of the enzyme–product complex.

Comparison of the rate constants (Table 2) shows that formation of primary complex proceeds approximately 10 times faster for cleavable substrates than for uncleavable ligands. Moreover, formation of the second complex proceeds approximately 2 orders of magnitude faster for DNA containing an AP site or DHU. The rate constants k_3 for FAM-AP-BHQ- and

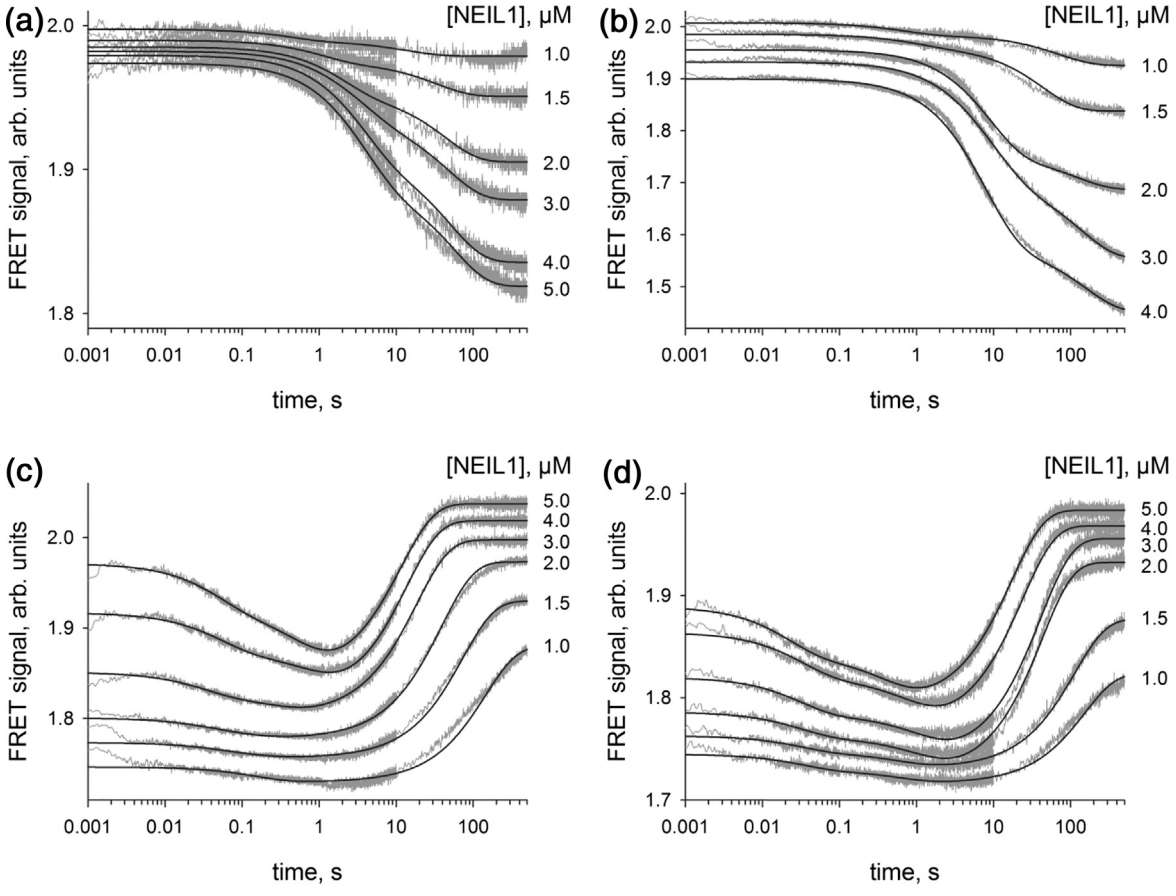

Fig. 5. Observed (jagged traces) and fitted (smooth curves) time courses of FRET signal changes during interaction of NEIL1 with undamaged DNA (a) and DNA containing the F-site (b), AP-site (c) and DHU base (d). The concentration of FRET duplexes was 1 μM. The concentration of NEIL1 is shown to the right of the panel.

$$\mathrm{E} + \mathrm{S} \underset{k_{-1}}{\overset{k_1}{\rightleftarrows}} \mathrm{ES1} \underset{k_{-2}}{\overset{k_2}{\rightleftarrows}} \mathrm{ES2} \overset{k_3}{\rightarrow} \mathrm{E} + \mathrm{P}$$

Scheme 5. Recognition of damaged DNA by NEIL1 as detected by FRET.

FAM-DHU-BHQ-substrates were similar, 0.11 and 0.07 s^{-1}, respectively, and closely coincided with the rate constant for catalysis calculated using Trp fluorescence changes (0.10 and 0.08 s^{-1}). These results indicate that β,δ-elimination is the rate-limiting step of the whole enzymatic process.

Discussion

Structural basis of Trp fluorescence in NEIL1

The complex sequence of events leading to base excision by H2TH superfamily enzymes emerges from a series of their structures representing several snapshots along the reaction path [25,27,28,30–35,38,54–57] in conjunction with molecular dynamic models connecting these snapshots [32,34,47,54,55,58–61] and stopped-flow fluorescence studies of *E. coli* Fpg and Nei [39–47]. The most likely order, proposed primarily from the data on Fpg, starts with non-specific DNA binding by the enzyme, followed by insertion of a wedge into the DNA stack, DNA kinking, eversion of the damaged nucleotide, insertion of "plugging" residues to fill the void left in the stack, and adjustment of the active site to the catalytically competent conformation. For human NEIL1, the available structures include the free enzyme and the enzyme bound to DNA containing an F-nucleotide or thymine glycol (Tg), thus representing the end points of the recognition process [29,38,62].

Changes in the fluorescence of proteins are mostly due to changes in the environment of their Trp residues, which, of all amino acids, have the highest fluorescence quantum yield. In practice, if no extensive rearrangement of protein residues surrounding the Trp indole groups occurs, changes in its fluorescence upon binding DNA usually reflect changes in Trp solvent exposure [63]. Human NEIL1 contains four Trp residues (Fig. 6, Supplementary Figs. 1 and 2), one of which, Trp122, is buried inside the N-terminal domain (Table S1). Three other Trp residues are well exposed and located in the protein elements that may be expected to show dynamics upon DNA binding: Trp128 is found in the inter-domain linker, Trp258, in the "missing loop" motif, which likely forms part of the lesion-binding pocket,

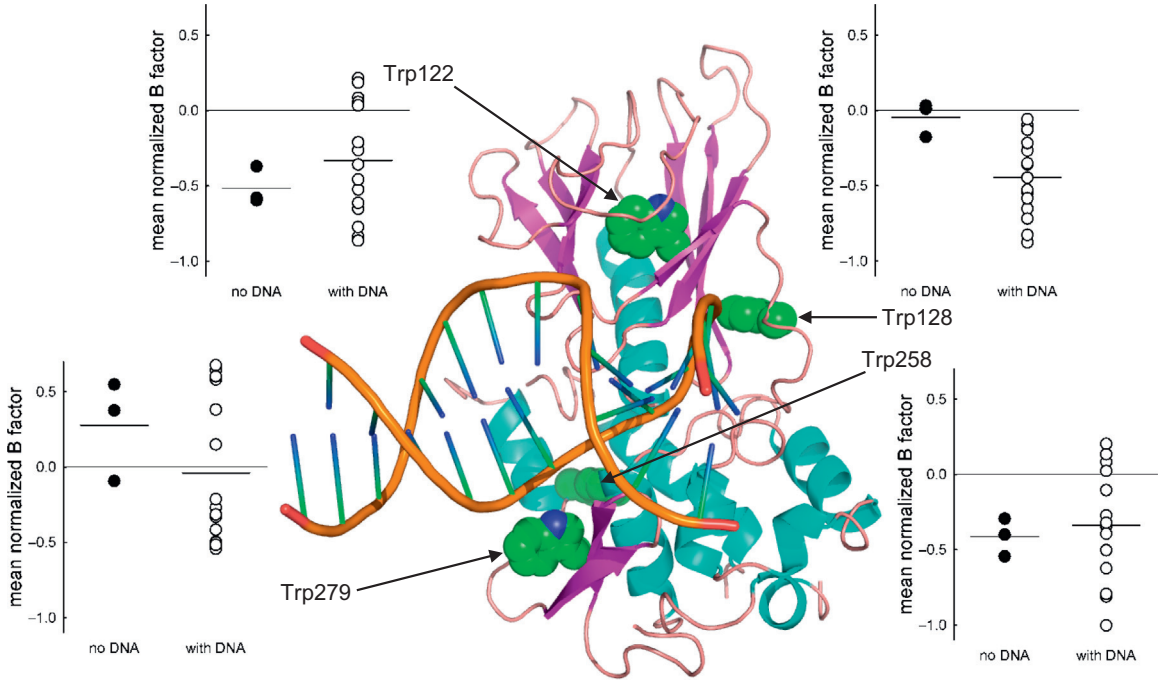

Fig. 6. Structure of NEIL1 bound to F-containing DNA (PDB ID 5ITU [38]). Trp side chains are shown as sphere models. Insets show the mobility of Trp environment, each dot corresponds to one protein chain in the PDB structures (see main text for detail). Mean normalized B-factor was calculated as $\overline{b_{5\text{Å}}} = \frac{\sum(B_{5\text{Å}} - \overline{B})}{n_{5\text{Å}}\sigma(B)}$, where $B_{5\text{Å}}$ is a *B*-factor for an atom within 5 Å of a Trp residue, $n_{5\text{Å}}$ is the number of such atoms, $\overline{B}$ is the mean *B*-factor for the whole protein, and $\sigma(B)$ is the standard deviation of the *B*-factor for the whole protein.

and Trp279, in the "zincless finger" DNA-binding motif (Fig. 6).

In order to attribute the observed fluorescence changes to particular Trp residues, we have analyzed all available structures of free NEIL1 (three protein chains in three structures; PDB ID 1TDH [29], 4NRV [62], and 5ITQ [38]), and NEIL1 bound to F-containing DNA (nine chains in three structures; PDB ID 5ITR, 5ITT, and 5ITU [38]) or Tg-containing DNA (6 chains in 2 structures; PDB ID 5ITX and 5ITY [38]). The structures of free and DNA-bound NEIL1 are essentially identical, with the gross movement restricted to a ~10° twisting rotation of N- and C-terminal domains centered around residues Pro130-Gly131 in the interdomain linker. Differences in the solvent-accessible area of Trp side chains were minimal, on the order of 2–3 Å^2 (Table S1), and could hardly explain the fluorescence dynamics. However, when we compared the mobility of the Trp side chain environment by averaging normalized B-factors of atoms within 5 Å of them, Trp128 was in a significantly more mobile environment (p = 0.024, Mann–Whitney test) in the free protein compared with DNA-bound NEIL1 (Fig. 6 and Table S1). The environment of Trp279 also tended to become less mobile upon DNA binding, albeit the difference did not reach statistical significance (Fig. 6 and Table S1). No significant differences between F- and Tg-bound NEIL1 were observed for any Trp. Higher mobility or Trp surroundings in proteins is usually associated with more efficient fluorescence quenching or spectral shift by solutes and other protein moieties [63,64], so the observed decreases in Trp fluorescence upon binding all four types of DNA (Figs. 1–4) agree well with a more dynamic environment of Trp128 and possibly Trp279. It should be emphasized that due to the difference in Trp location in NEIL1, Fpg and Nei (Supplementary Figs. 1 and 2), similar structural changes in these proteins may have different impact on the Trp fluorescence curves.

Comparison of dynamics revealed by Trp fluorescence and FRET

For easier comparison of fluorescently discernible steps with different kinds of DNA, we have modeled the flow of enzyme–DNA species through the reaction using the Monte Carlo approach [65,66] with the experimentally determined rate constants. As shown in Fig. 7, the first Trp complex peaked at approximately the same time for all kinds of DNA. The uncleavable ligands then proceeded to the second Trp complex with a nearly indistinguishable kinetics. The AP- and DHU-substrates formed the ES2 complex also quite synchronously but then the base-containing DHU substrate lagged behind its abasic counterpart, with the lag persisting until the final product formation. This was due to intrusion of an additional intermediate, ES3, in the reaction scheme for DHU, so that the last pre-catalytic complex, ES4, was equivalent to ES3 in the reaction scheme for the AP-substrate (Fig. 7). Notably, while EL2 for both G- and F-ligand preferably partitioned back to EL1, ES2 for both AP- and especially DHU-substrate efficiently partitioned forward and accumulated later in time than EL2 (Table 1, Fig. 7), indicating that EL2 and ES2 may be structurally different.

The dynamics of intermediates discernible by FRET corroborated the suggestion that EL and ES complexes diverge in their structure. ES1^{FRET} complexes for AP- and DHU-substrate appeared between ES1^{Trp} to ES2^{Trp}, and were followed by ES2^{FRET} in transit from ES2^{Trp} to the pre-catalytic complex (ES3^{Trp} for the AP-substrate and ES4^{Trp} for the DHU-substrate). EL1^{FRET} intermediates emerged later than ES1^{FRET} ones, and EL2^{FRET} complexes were detectable only after prolonged time, comparable with the full reaction time for the substrates. Product formation was detected by FRET at longer times compared with Trp, apparently because additional time is required for duplex dissociation and separation of FAM and BHQ1 (Fig. 7).

Structural features of lesion recognition by NEIL1

Since only the structures of free NEIL1 and NEIL1 bound to base-containing and abasic lesions are known, the relevant conformational features of the recognition intermediates have to be inferred. The recognition scheme proposed for NEIL1 is summarized in Fig. 8. All DNA glycosylases insert several residues into the DNA helix to disrupt the target base pair stacking and stabilize the lesion in the extrahelical position. In NEIL1, Phe119 wedges between the target base pair and the base pair 3′ to it (counting along the damaged strand), Arg117 forms hydrogen bonds to the orphaned base, and Met80 fills the void formed after the damaged nucleotide eversion [38]; in *E. coli*, Fpg, Phe110, Arg108 and Met73 are their counterparts [26]. Also, all DNA glycosylases kink the DNA axis by >40° to facilitate the eversion of the target nucleotide. The earliest reaction step observed by Trp fluorescence occurs within milliseconds in all NEIL1–DNA complexes, as well as in *E. coli* Fpg and Nei (Figs. 1–4), and most likely reflects formation of the "primary" complex common for both normal and damaged DNA. Although no structure of any H2TH enzyme for this very early intermediate is available, experiments with Fpg processing DNA with internal and terminal fluorescent labels unambiguously show that at this stage DNA is not kinked, and the wedge intercalation is yet to occur [41,47]. The similarity of the first Trp- and FRET-discernible stages between NEIL1 and

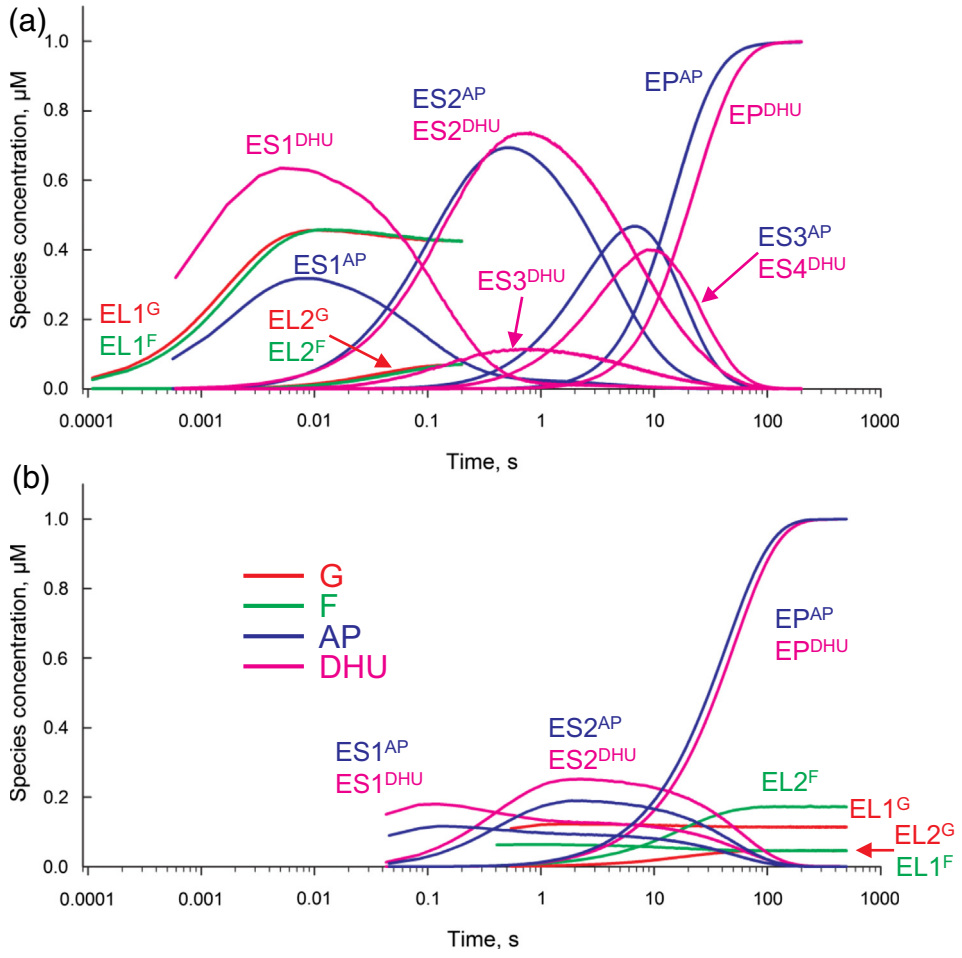

Fig. 7. Concentration of enzyme–DNA intermediates in modeled NEIL1 interactions with different ligands or substrates. (a) Species detected by Trp fluorescence. (b) Species detected by FRET. The labels are color-matched to the nature of DNA (panel b). The initial concentrations of NEIL1 and DNA in the model were 1 μM. The simulation was run for 0.2 s for G- and F-ligand Trp-detected species, 200 s for AP- and DHU-substrate Trp-detected species, and 500 s for FRET models.

Fpg (Figs. 1b–4b) suggests that the NEIL1 primary complex shares the same structural features.

The order of kinking and intercalation at the earlies steps of base sampling is not established unambiguously for any DNA glycosylase, for the lack of structures of primary encounter complexes. For H2TH superfamily enzymes, in the structure of the F113A mutant of *Geobacillus stearothermophilus*

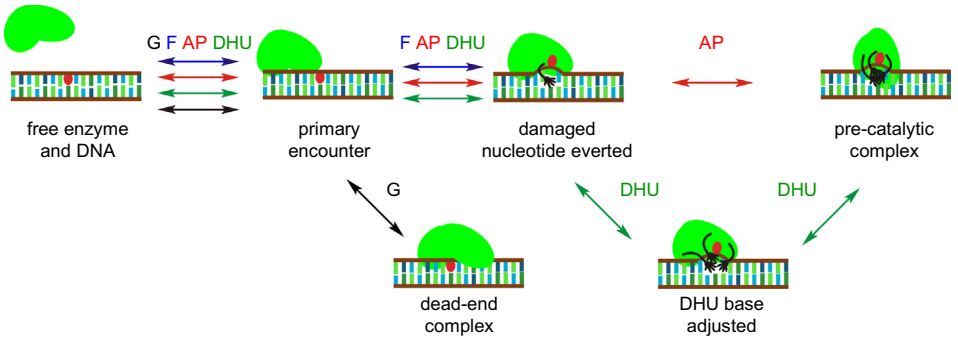

Fig. 8. General scheme for NEIL1 recognition of normal and damaged DNA. For Nei, the same principal scheme is suggested with the only difference being the lack of the additional adjustment step for DHU [45,48].

Table 1. Rate and equilibrium constants of the interaction of NEIL1 with DNA obtained by analysis of Trp fluorescence traces

Constant	G-ligand	F-ligand	AP-substrate	DHU-substrate
k_1, $M^{-1} \times s^{-1}$	(300 ± 40) × 10^6	(250 ± 30) × 10^6	(180 ± 30) × 10^6	(840 ± 60) × 10^6
k_{-1}, s^{-1}	180 ± 10	150 ± 30	210 ± 20	140 ± 40
k_2, s^{-1}	4.1 ± 1.5	3.9 ± 1.0	20 ± 1	9.4 ± 1.4
k_{-2}, s^{-1}	25 ± 1	17 ± 1	0.7 ± 0.1	0.15 ± 0.03
k_3, s^{-1}			0.26 ± 0.01	14 ± 1
k_{-3}, s^{-1}			0.016 ± 0.002	90 ± 10
k_4, s^{-1}			0.10 ± 0.01	1.0 ± 0.2
k_{-4}, s^{-1}			–	0.04 ± 0.01
k_5, s^{-1}			–	0.08 ± 0.01
K_{bind}[a], M^{-1}	(2.0 ± 0.3) × 10^6	(2.2 ± 0.6) × 10^6	(4.5 ± 0.5) × 10^8	(1.0 ± 0.7) × 10^9
K_M[b], M			(3.7 ± 0.8) × 10^{-8}	(1.8 ± 0.7) × 10^{-9}
k_{cat}[b], s^{-1}			0.066 ± 0.005	0.040 ± 0.005
K_P, M			(3.6 ± 0.1) × 10^{-6}	(1.1 ± 0.3) × 10^{-6}

[a] For n-step binding, $K_{bind} = \sum_{i=1}^{N} \prod_{j=1}^{j=i} K_j, K_j = \frac{k_j}{k_{-j}}$

[b] Calculated from the rate constants using kinetic graph theory:
For three-step binding, $K_M = A/k_1B$, $k_{cat} = k_2k_3k_4/B$, where
$A = k_{-1}\,k_{-2}\,k_{-3} + k_{-1}\,k_{-2}\,k_4 + k_{-1}k_3k_4 + k_2k_3k_4$ and
$B = k_{-2}\,k_{-3} + k_{-2}\,k_4 + k_3k_4 + k_2k_{-3} + k_2k_4 + k_2k_3$.
For four-step binding, $K_M = A/k_1B$, $k_{cat} = k_2k_3k_4k_5/B$, where
$A = k_{-1}k_{-2}k_{-3}\,k_{-4} + k_{-1}k_{-2}k_{-3}\,k_5 + k_{-1}k_{-2}k_4k_5 + k_{-1}k_3k_4k_5 + k_2k_3k_4k_5$ and
$B = k_{-2}k_{-3}\,k_{-4} + k_{-2}k_{-3}\,k_5 + k_{-2}k_4k_5 + k_3k_4k_5 + k_2k_{-3}\,k_{-4} + k_2k_{-3}\,k_5 + k_2k_4k_5 + k_2k_3k_5 + k_2k_3k_{-4} + k_2k_3k_4$.

Fpg the kinking angle of both G- and oxoG-containing DNA is indistinguishable from the complexes with the Phe wedge present [57]. In the FRET studies of *E. coli* Fpg F110A, the initial kinking also proceeds with the same kinetics in both the wild-type and the mutant enzyme [47].Here, the first FRET complex with AP and DHU substrates also occurs between Trp-detectable ES1 and ES2 (Fig. 7). On the other hand, kinking by Fpg occurs later in time than stacking disruption detected by fluorescence of reporter DNA bases 2-aminopurine and pyrrolocytosine [44,47]. Altogether, it seems that wedge intercalation precedes DNA kinking but does not drive this process, at least in Fpg and possibly in NEIL1.

A comparison of F-ligand and AP-substrate processing by NEIL1 reveals more similarities with Nei than with Fpg [40,41,45]. In Fpg, AP site cleavage essentially continues a conformational path common for F and AP lesions, adding a single irreversible step and enzyme–product equilibrium to the reaction scheme. In NEIL1 and Nei, AP site cleavage requires an additional reversible stage, and the rate constants for the second Trp-detected equilibrium were quite different from those observed for F-ligand binding. Thus, as suggested for Nei [45,48], the kinetic discrimination between AP and F may start at early stages of the reaction. The differences in FRET-discernible species flow between the F-ligand and the AP-substrate are also in agreement with this proposal. The structural reason for the differences in binding F and AP site may lie in the interaction between the α-amino group of the N-terminal Pro1 and the hydroxyl at C1′, which is absent from F.

Notably, despite the similarities of the kinetic schemes and constants for G- and F-ligands, these processes evidently proceed through different conformational pathways (Fig. 8). Binding of the G-ligand is accompanied with a decrease followed by an increase in the Trp signal, whereas F-ligand is bound in two steps of decreasing Trp fluorescence. Since the final structure of NEIL1:F-DNA complex contains fully everted F nucleotide and all three intercalating residues in place, one may assume that the second Trp-discernible step reflects intercalation and eversion. Then NEIL1 is probably unable to efficiently invade undamaged DNA, which quickly induces some non-productive conformation after the initial encounter. Such behavior is consistent with the active destabilization model of damage sensing proposed earlier for Fpg [32,47,67] and is not easily reconciled with an alternative model of selective binding of pre-everted damaged nucleotides suggested for uracil-DNA glycosylase, an enzyme from another structural superfamily [68]. We also note that since NEIL1 scans and samples non-specific DNA in search of the lesions, it is likely that binding in several registers and orientations will occur with similar affinity in the stopped-flow experiments. Thus, the binding curves for unmodified DNA reflect some "averaged" microscopic binding constant rather than the binding constant for a single specifically recognized nucleotide pair.

Finally, when the damaged base was present in the substrate, an extra intermediate was present in

Table 2. Rate and equilibrium constants of the interaction of NEIL1 with DNA obtained by analysis of FRET traces

Constant	FAM-C-BHQ	FAM-F-BHQ	FAM-AP-BHQ	FAM-DHU-BHQ
k_1, $M^{-1} \times s^{-1}$	$(0.5 \pm 0.2) \times 10^6$	$(0.6 \pm 0.4) \times 10^6$	$(3.6 \pm 1.1) \times 10^6$	$(7.0 \pm 2.0) \times 10^6$
k_{-1}, s^{-1}	3.1 ± 1.8	8.0 ± 5.0	18.8 ± 5.6	20 ± 9
k_2, s^{-1}	0.02 ± 0.01	0.15 ± 0.06	3.7 ± 0.7	3.3 ± 1.8
k_{-2}, s^{-1}	0.05 ± 0.02	0.04 ± 0.01	1.7 ± 0.2	1.6 ± 0.9
k_3, s^{-1}	–	–	0.11 ± 0.02	0.07 ± 0.02
K_{bind}[a], M^{-1}	$(3.9 \pm 0.6) \times 10^5$	$(3.6 \pm 0.7) \times 10^5$	$(5.6 \pm 0.5) \times 10^5$	$(9.0 \pm 2.0) \times 10^5$

[a] $K_{bind} = K_1 + K_1 \times K_2$, where $K_i = k_i/k_{-i}$.

the NEIL1 kinetic scheme compared with the AP-substrate. A similar situation was also observed for Fpg excising 8-oxoguanine [40]; notably, in that case, the additional step clearly followed the steps present in the cleavage of the AP-substrate, significantly slowed down the reaction, and was attributed to the conformational adjustment of the base-binding pocket. Neither Nei nor Fpg displayed this additional step when cleaving the DHU-substrate [41,45]. In NEIL1, the additional step ostensibly appeared before the last reversible step (thus likely reflecting some features of nucleotide eversion not present in the abasic DNA), and the overall reaction time was extended only ~2-fold (Fig. 7). This result supports the idea that the non-planar DHU base partly destabilizes DNA duplex and is easily everted, having only a minor effect on the overall rate of the enzymatic reaction. Overall, NEIL1 generally follows the same recognition pathway as Nei but contains an additional step of damaged base adjustment in the enzyme's active site (Fig. 8).

Our results with NEIL1 fit the general picture of DNA glycosylases as enzymes that initiate damage recognition through indirect readout, probing DNA for flexibility or other conformational response to the strain induced upon enzyme binding, and using direct contacts with the damaged base only at later stages of the reaction to confirm the presence of the lesion. A complete dissection of the conformational pathway of damage recognition by NEIL1 protein will require studies with a series of fluorescence reporters, site-directed mutants, and an extended range of substrates, and should illuminate the reasons behind the marked preference for different DNA structures demonstrated by enzymes of H2TH structural superfamily.

Table 3. Sequences of oligodeoxynucleotides used in this study[a]

Shorthand	Sequence
X/Y	C T C T C **X** C C T T C C
X = G, F, AP, DHU	G A G A G **Y** G G A A G G
Y = C opposite G	
Y = G in other cases	
FAM-X-BHQ	FAM-G C T C A **X** G T A C A G A G C T G
X = C, F, AP, DHU	C G A G T G C A T G T C T C G A C-BHQ1

[a] FAM is 6-carboxyfluorescein, BHQ1 is Black Hole Quencher 1.

Materials and Methods

Oligonucleotides and enzymes

Oligodeoxyribonucleotides listed in Table 3 were synthesized in-house from commercially available phosphoramidites (Glen Research, Sterling, VA) and purified by reverse-phase HPLC. To prepare the AP-substrate, the oligonucleotide containing a single deoxyuridine residue was treated with *E. coli* uracil–DNA glycosylase (New England Biolabs, Beverly, MA) and purified by reverse-phase HPLC as in Ref. [69]. DNA duplexes were prepared by annealing equimolar amounts of the modified and complementary strands. Full-length human NEIL1 protein was overproduced in *E. coli* BL21(DE3) and purified as described [13]. The fraction of the active enzyme (~80%) was determined by reductive cross-linking to radioactively labeled AP-substrate [70].

Stopped-flow experiments

Stopped-flow measurements with fluorescence detection were carried out essentially as described [40,45,50]. A model SX.18MV stopped-flow spectrometer (Applied Photophysics, Leatherhead, UK) fitted with a 150-W Xe arc lamp and a 2-mm path length optical cell was used. The dead time of the instrument was 1.4 ms. Experiments were performed at 25 °C in the buffer containing 50 mM Tris–HCl (pH 7.5), 50 mM KCl, 9% (v/v) glycerol, 1 mM ethylenediamine tetraacetate and 1 mM dithiothreitol. The fluorescence of Trp was excited at λ_{ex} = 290 nm and monitored at $\lambda_{em} > 320$ nm as transmitted by the WG-320 filter (Schott, Mainz, Germany). If 6-carboxyfluorescein (FAM) was present in the duplex, the wavelength λ_{ex} = 494 nm was used to excite the fluorophore, and the emission was recorded at $\lambda_{em} > 515$ nm (Schott filter OG-515).

The enzyme was placed in one syringe of the instrument and rapidly mixed in the reaction chamber with the substrate from another syringe. The concentrations of NEIL1 and DNA substrates in the

reaction chamber after mixing are specified everywhere in the text. In the figures, if necessary for better visibility, the curves were manually moved apart.

Pre-steady-state kinetic parameters for possible kinetic schemes were determined by global non-linear fitting using DynaFit 4 software (BioKin, Pullman, WA) [71] as described previously [42–44,46,51]. Several kinetic schemes were considered, with the minimal scheme selected based on the residuals *versus* number of steps test [41]. Kinetic simulation of the time course of appearance and disappearance of different reaction intermediates was done by solving the system of differential equations using DynaFit and by Monte Carlo modeling using Kinetiscope v1.1 (Columbia Hill Technical Consulting, Fremont, CA) with essentially identical results. In the Monte Carlo modeling, the system included 10^6 particles at 298.15 K, initially equally distributed between free NEIL1 and DNA.

Structural analysis

All available structures of free and DNA-bound human NEIL1 (1TDH [29], 4NRV [62], 5ITQ, 5ITR, 5ITT, 5ITU, 5ITX, 5ITY [38]) were analyzed for the environment of the Trp residues. Solvent-accessible surface area (1.4 Å probe) was calculated using GETAREA [72].

Acknowledgments

This research was supported partially by Russian State-funded budget projects VI.57.1.2 0309-2018-0001 (O.A.K., O.S.F., N.A.K.), VI.62.1.5 0309-2018-0003 (I.R.G. and D.O.Z.) and 6.5773.2017/6.7 (D.O.Z.). The part of the work including Trp stopped-flow analysis and computational studies was supported by the Russian Science Foundation (Grant 17-14-01190; to D.O.Z.). The part of the work including FRET stopped-flow analysis was supported by the Russian Science Foundation (Grant 18-14-00135; to N.A.K.). Russian Foundation for Basic Research (19-04-00012 to O.S.F., 18-44-540029 joint RFBR and Novosibirsk Region to I.R.G.) is also acknowledged.

Appendix A. Supplementary data

Supplementary data to this article can be found online at https://doi.org/10.1016/j.jmb.2019.01.030.

Received 4 December 2018;
Received in revised form 23 January 2019;
Accepted 23 January 2019
Available online 1 February 2019

Keywords:
DNA repair;
DNA glycosylase;
NEIL1;
substrate recognition;
stopped-flow kinetics

†O.A.K. and I.R.G. contributed equally to this work.

Abbreviations used:
AP, apurinic/apyrimidinic; DHU, 5,6-dihydrouracil; F, (3-hydroxytetrahydrofuran-2-yl)methyl phosphate; FRET, Förster resonance energy transfer.

References

[1] C. von Sonntag, Free-Radical-Induced DNA Damage and Its Repair: A Chemical Perspective, Springer, Berlin–Heidelberg, 2006.
[2] B. Halliwell, J.M.C. Gutteridge, Free Radicals in Biology and Medicine, Oxford University Press, Oxford, 2007.
[3] S.S. Wallace, Biological consequences of free radical-damaged DNA bases, Free Radic. Biol. Med. 33 (2002) 1–14, https://doi.org/10.1016/S0891-5849(02)00827-4.
[4] M.D. Evans, M. Dizdaroglu, M.S. Cooke, Oxidative DNA damage and disease: induction, repair and significance, Mutat. Res. 567 (2004) 1–61, https://doi.org/10.1016/j.mrrev.2003.11.001.
[5] E.C. Friedberg, G.C. Walker, W. Siede, R.D. Wood, R.A. Schultz, T. Ellenberger, DNA Repair and Mutagenesis, ASM Press, Washington, DC, 2006.
[6] D.O. Zharkov, Base excision DNA repair, Cell. Mol. Life Sci. 65 (2008) 1544–1565, https://doi.org/10.1007/s00018-008-7543-2.
[7] D.O. Zharkov, G. Shoham, A.P. Grollman, Structural characterization of the Fpg family of DNA glycosylases, DNA Repair 2 (2003) 839–862, https://doi.org/10.1016/S1568-7864(03)00084-3.
[8] A. Prakash, S. Doublié, S.S. Wallace, The Fpg/Nei family of DNA glycosylases: substrates, structures, and search for damage, Prog. Mol. Biol. Transl. Sci. 110 (2012) 71–91, https://doi.org/10.1016/B978-0-12-387665-2.00004-3.
[9] S.S. Wallace, V. Bandaru, S.D. Kathe, J.P. Bond, The enigma of endonuclease VIII, DNA Repair 2 (2003) 441–453, https://doi.org/10.1016/S1568-7864(02)00182-9.
[10] T.K. Hazra, T. Izumi, I. Boldogh, B. Imhoff, Y.W. Kow, P. Jaruga, M. Dizdaroglu, S. Mitra, Identification and characterization of a human DNA glycosylase for repair of modified bases in oxidatively damaged DNA, Proc. Natl. Acad. Sci. U. S. A. 99 (2002) 3523–3528, https://doi.org/10.1073/pnas.062053799.
[11] I. Morland, V. Rolseth, L. Luna, T. Rognes, M. Bjørås, E. Seeberg, Human DNA glycosylases of the bacterial Fpg/MutM superfamily: an alternative pathway for the repair of 8-oxoguanine and other oxidation products in DNA, Nucleic Acids Res. 30 (2002) 4926–4936, https://doi.org/10.1093/nar/gkf618.
[12] T.A. Rosenquist, E. Zaika, A.S. Fernandes, D.O. Zharkov, H. Miller, A.P. Grollman, The novel DNA glycosylase, NEIL1, protects mammalian cells from radiation-mediated cell death, DNA Repair 2 (2003) 581–591, https://doi.org/10.1016/S1568-7864(03)00025-9.

[13] A. Katafuchi, T. Nakano, A. Masaoka, H. Terato, S. Iwai, F. Hanaoka, H. Ide, Differential specificity of human and *Escherichia coli* endonuclease III and VIII homologues for oxidative base lesions, J. Biol. Chem. 279 (2004) 14464–14471, https://doi.org/10.1074/jbc.M400393200.
[14] P. Jaruga, M. Birincioglu, T.A. Rosenquist, M. Dizdaroglu, Mouse NEIL1 protein is specific for excision of 2,6-diamino-4-hydroxy-5-formamidopyrimidine and 4,6-diamino-5-formamidopyrimidine from oxidatively damaged DNA, Biochemistry 43 (2004) 15909–15914, https://doi.org/10.1021/bi048162l.
[15] I.R. Grin, G.L. Dianov, D.O. Zharkov, The role of mammalian NEIL1 protein in the repair of 8-oxo-7,8-dihydroadenine in DNA, FEBS Lett. 584 (2010) 1553–1557, https://doi.org/10.1016/j.febslet.2010.03.009.
[16] T.K. Hazra, Y.W. Kow, Z. Hatahet, B. Imhoff, I. Boldogh, S.K. Mokkapati, S. Mitra, T. Izumi, Identification and characterization of a novel human DNA glycosylase for repair of cytosine-derived lesions, J. Biol. Chem. 277 (2002) 30417–30420, https://doi.org/10.1074/jbc.C200355200.
[17] H. Dou, S. Mitra, T.K. Hazra, Repair of oxidized bases in DNA bubble structures by human DNA glycosylases NEIL1 and NEIL2, J. Biol. Chem. 278 (2003) 49679–49684, https://doi.org/10.1074/jbc.M308658200.
[18] M. Redrejo-Rodríguez, C. Saint-Pierre, S. Couve, A. Mazouzi, A.A. Ishchenko, D. Gasparutto, M. Saparbaev, New insights in the removal of the hydantoins, oxidation product of pyrimidines, via the base excision and nucleotide incision repair pathways, PLoS One 6 (2011), e21039. https://doi.org/10.1371/journal.pone.0021039.
[19] S.Z. Krokeide, J.K. Laerdahl, M. Salah, L. Luna, F.H. Cederkvist, A.M. Fleming, C.J. Burrows, B. Dalhus, M. Bjørås, Human NEIL3 is mainly a monofunctional DNA glycosylase removing spiroimindiohydantoin and guanidinohydantoin, DNA Repair 12 (2013) 1159–1164, https://doi.org/10.1016/j.dnarep.2013.04.026.
[20] M. Liu, S. Doublié, S.S. Wallace, Neil3, the final frontier for the DNA glycosylases that recognize oxidative damage, Mutat. Res. 743-744 (2013) 4–11, https://doi.org/10.1016/j.mrfmmm.2012.12.003.
[21] A.K. McCullough, M.L. Dodson, R.S. Lloyd, Initiation of base excision repair: glycosylase mechanisms and structures, Annu. Rev. Biochem. 68 (1999) 255–285, https://doi.org/10.1146/annurev.biochem.68.1.255.
[22] J. Tchou, A.P. Grollman, The catalytic mechanism of Fpg protein: evidence for a Schiff base intermediate and amino terminus localization of the catalytic site, J. Biol. Chem. 270 (1995) 11671–11677, https://doi.org/10.1074/jbc.270.19.11671.
[23] R.A. Rieger, M.M. McTigue, J.H. Kycia, S.E. Gerchman, A.P. Grollman, C.R. Iden, Characterization of a cross-linked DNA-endonuclease VIII repair complex by electrospray ionization mass spectrometry, J. Am. Soc. Mass Spectrom. 11 (2000) 505–515, https://doi.org/10.1016/S1044-0305(00)00117-3.
[24] E.S. Vik, I. Alseth, M. Forsbring, I.H. Helle, I. Morland, L. Luna, M. Bjørås, B. Dalhus, Biochemical mapping of human NEIL1 DNA glycosylase and AP lyase activities, DNA Repair 11 (2012) 766–773, https://doi.org/10.1016/j.dnarep.2012.07.002.
[25] D.O. Zharkov, G. Golan, R. Gilboa, A.S. Fernandes, S.E. Gerchman, J.H. Kycia, R.A. Rieger, A.P. Grollman, G. Shoham, Structural analysis of an *Escherichia coli* endonuclease VIII covalent reaction intermediate, EMBO J. 21 (2002) 789–800, https://doi.org/10.1093/emboj/21.4.789.
[26] R. Gilboa, D.O. Zharkov, G. Golan, A.S. Fernandes, S.E. Gerchman, E. Matz, J.H. Kycia, A.P. Grollman, G. Shoham, Structure of formamidopyrimidine-DNA glycosylase covalently complexed to DNA, J. Biol. Chem. 277 (2002) 19811–19816, https://doi.org/10.1074/jbc.M202058200.
[27] J.C. Fromme, G.L. Verdine, Structural insights into lesion recognition and repair by the bacterial 8-oxoguanine DNA glycosylase MutM, Nat. Struct. Biol. 9 (2002) 544–552, https://doi.org/10.1038/nsb809.
[28] J.C. Fromme, G.L. Verdine, DNA lesion recognition by the bacterial repair enzyme MutM, J. Biol. Chem. 278 (2003) 51543–51548, https://doi.org/10.1074/jbc.M307768200.
[29] S. Doublié, V. Bandaru, J.P. Bond, S.S. Wallace, The crystal structure of human endonuclease VIII-like 1 (NEIL1) reveals a zincless finger motif required for glycosylase activity, Proc. Natl. Acad. Sci. U. S. A. 101 (2004) 10284–10289, https://doi.org/10.1073/pnas.0402051101.
[30] G. Golan, D.O. Zharkov, H. Feinberg, A.S. Fernandes, E.I. Zaika, J.H. Kycia, A.P. Grollman, G. Shoham, Structure of the uncomplexed DNA repair enzyme endonuclease VIII indicates significant interdomain flexibility, Nucleic Acids Res. 33 (2005) 5006–5016, https://doi.org/10.1093/nar/gki796.
[31] A. Banerjee, W.L. Santos, G.L. Verdine, Structure of a DNA glycosylase searching for lesions, Science 311 (2006) 1153–1157, https://doi.org/10.1126/science.1120288.
[32] Y. Qi, M.C. Spong, K. Nam, A. Banerjee, S. Jiralerspong, M. Karplus, G.L. Verdine, Encounter and extrusion of an intrahelical lesion by a DNA repair enzyme, Nature 462 (2009) 762–766, https://doi.org/10.1038/nature08561.
[33] K. Imamura, S.S. Wallace, S. Doublié, Structural characterization of a viral NEIL1 ortholog unliganded and bound to abasic site-containing DNA, J. Biol. Chem. 284 (2009) 26174–26183, https://doi.org/10.1074/jbc.M109.021907.
[34] Y. Qi, M.C. Spong, K. Nam, M. Karplus, G.L. Verdine, Entrapment and structure of an extrahelical guanine attempting to enter the active site of a bacterial DNA glycosylase, MutM, J. Biol. Chem. 285 (2010) 1468–1478, https://doi.org/10.1074/jbc.M109.069799.
[35] K. Imamura, A. Averill, S.S. Wallace, S. Doublié, Structural characterization of viral ortholog of human DNA glycosylase NEIL1 bound to thymine glycol or 5-hydroxyuracil-containing DNA, J. Biol. Chem. 287 (2012) 4288–4298, https://doi.org/10.1074/jbc.M111.315309.
[36] A. Prakash, B.E. Eckenroth, A.M. Averill, K. Imamura, S.S. Wallace, S. Doublié, Structural investigation of a viral ortholog of human NEIL2/3 DNA glycosylases, DNA Repair 12 (2013) 1062–1071, https://doi.org/10.1016/j.dnarep.2013.09.004.
[37] M. Liu, K. Imamura, A.M. Averill, S.S. Wallace, S. Doublié, Structural characterization of a mouse ortholog of human NEIL3 with a marked preference for single-stranded DNA, Structure 21 (2013) 247–256, https://doi.org/10.1016/j.str.2012.12.008.
[38] C. Zhu, L. Lu, J. Zhang, Z. Yue, J. Song, S. Zong, M. Liu, O. Stovicek, Y.Q. Gao, C. Yi, Tautomerization-dependent recognition and excision of oxidation damage in base-excision DNA repair, Proc. Natl. Acad. Sci. U. S. A. 113 (2016) 7792–7797, https://doi.org/10.1073/pnas.1604591113.
[39] O.S. Fedorova, G.A. Nevinsky, V.V. Koval, A.A. Ishchenko, N.L. Vasilenko, K.T. Douglas, Stopped-flow kinetic studies of the interaction between *Escherichia coli* Fpg protein and DNA substrates, Biochemistry 41 (2002) 1520–1528, https://doi.org/10.1021/bi011524u.
[40] V.V. Koval, N.A. Kuznetsov, D.O. Zharkov, A.A. Ishchenko, K.T. Douglas, G.A. Nevinsky, O.S. Fedorova, Pre-steady-state kinetics shows differences in processing of various DNA lesions by *Escherichia coli* formamidopyrimidine-

DNA glycosylase, Nucleic Acids Res. 32 (2004) 926–935, https://doi.org/10.1093/nar/gkh237.
[41] N.A. Kuznetsov, V.V. Koval, D.O. Zharkov, Y.N. Vorobjev, G.A. Nevinsky, K.T. Douglas, O.S. Fedorova, Pre-steady-state kinetic study of substrate specificity of *Escherichia coli* formamidopyrimidine–DNA glycosylase, Biochemistry 46 (2007) 424–435, https://doi.org/10.1021/bi060787r.
[42] N.A. Kuznetsov, D.O. Zharkov, V.V. Koval, M. Buckle, O.S. Fedorova, Reversible chemical step and rate-limiting enzyme regeneration in the reaction catalyzed by formamidopyrimidine–DNA-glycosylase, Biochemistry 48 (2009) 11335–11343, https://doi.org/10.1021/bi901100b.
[43] V.V. Koval, N.A. Kuznetsov, A.A. Ishchenko, M.K. Saparbaev, O.S. Fedorova, Real-time studies of conformational dynamics of the repair enzyme *E. coli* formamidopyrimidine–DNA glycosylase and its DNA complexes during catalytic cycle, Mutat. Res. 685 (2010) 3–10, https://doi.org/10.1016/j.mrfmmm.2009.08.018.
[44] N.A. Kuznetsov, Y.N. Vorobjev, L.N. Krasnoperov, O.S. Fedorova, Thermodynamics of the multi-stage DNA lesion recognition and repair by formamidopyrimidine–DNA glycosylase using pyrrolocytosine fluorescence–stopped-flow pre-steady-state kinetics, Nucleic Acids Res. 40 (2012) 7384–7392, https://doi.org/10.1093/nar/gks423.
[45] N.A. Kuznetsov, V.V. Koval, D.O. Zharkov, O.S. Fedorova, Conformational dynamics of the interaction of *Escherichia coli* endonuclease VIII with DNA substrates, DNA Repair 11 (2012) 884–891, https://doi.org/10.1016/j.dnarep.2012.08.004.
[46] A.A. Kuznetsova, N.A. Kuznetsov, Y.N. Vorobjev, N.P.F. Barthes, B.Y. Michel, A. Burger, O.S. Fedorova, New environment-sensitive multichannel DNA fluorescent label for investigation of the protein–DNA interactions, PLoS One 9 (2014), e100007. https://doi.org/10.1371/journal.pone.0100007.
[47] N.A. Kuznetsov, C. Bergonzo, A.J. Campbell, H. Li, G.V. Mechetin, C. de los Santos, A.P. Grollman, O.S. Fedorova, D.O. Zharkov, C. Simmerling, Active destabilization of base pairs by a DNA glycosylase wedge initiates damage recognition, Nucleic Acids Res. 43 (2015) 272–281, https://doi.org/10.1093/nar/gku1300.
[48] O.A. Kladova, A.A. Kuznetsova, O.S. Fedorova, N.A. Kuznetsov, Mutational and kinetic analysis of lesion recognition by *Escherichia coli* endonuclease VIII, Genes 8 (2017) 140, https://doi.org/10.3390/genes8050140.
[49] D.O. Zharkov, A.P. Grollman, The DNA trackwalkers: principles of lesion search and recognition by DNA glycosylases, Mutat. Res. 577 (2005) 24–54, https://doi.org/10.1016/j.mrfmmm.2005.03.011.
[50] N.A. Kuznetsov, V.V. Koval, D.O. Zharkov, G.A. Nevinsky, K.T. Douglas, O.S. Fedorova, Kinetics of substrate recognition and cleavage by human 8-oxoguanine–DNA glycosylase, Nucleic Acids Res. 33 (2005) 3919–3931, https://doi.org/10.1093/nar/gki694.
[51] N.A. Kuznetsov, O.A. Kladova, A.A. Kuznetsova, A.A. Ishchenko, M.K. Saparbaev, D.O. Zharkov, O.S. Fedorova, Conformational dynamics of DNA repair by *Escherichia coli* endonuclease III, J. Biol. Chem. 290 (2015) 14338–14349, https://doi.org/10.1074/jbc.M114.621128.
[52] T.K. Hazra, S. Mitra, Purification and characterization of NEIL1 and NEIL2, members of a distinct family of mammalian DNA glycosylases for repair of oxidized bases, Methods Enzymol. 408 (2006) 33–48, https://doi.org/10.1016/S0076-6879(06)08003-7.
[53] N.A. Kuznetsov, V.V. Koval, G.A. Nevinsky, K.T. Douglas, D.O. Zharkov, O.S. Fedorova, Kinetic conformational analysis of human 8-oxoguanine–DNA glycosylase, J. Biol. Chem. 282 (2007) 1029–1038, https://doi.org/10.1074/jbc.M605788200.
[54] K. Nam, G.L. Verdine, M. Karplus, Analysis of an anomalous mutant of MutM DNA glycosylase leads to new insights into the catalytic mechanism, J. Am. Chem. Soc. 131 (2009) 18208–18209, https://doi.org/10.1021/ja907544b.
[55] Y. Qi, K. Nam, M.C. Spong, A. Banerjee, R.-J. Sung, M. Zhang, M. Karplus, G.L. Verdine, Strandwise translocation of a DNA glycosylase on undamaged DNA, Proc. Natl. Acad. Sci. U. S. A. 109 (2012) 1086–1091, https://doi.org/10.1073/pnas.1111237108.
[56] R.-J. Sung, M. Zhang, Y. Qi, G.L. Verdine, Sequence-dependent structural variation in DNA undergoing intrahelical inspection by the DNA glycosylase MutM, J. Biol. Chem. 287 (2012) 18044–18054, https://doi.org/10.1074/jbc.M111.313635.
[57] R.-J. Sung, M. Zhang, Y. Qi, G.L. Verdine, Structural and biochemical analysis of DNA helix invasion by the bacterial 8-oxoguanine DNA glycosylase MutM, J. Biol. Chem. 288 (2013) 10012–10023, https://doi.org/10.1074/jbc.M112.415612.
[58] K. Song, V. Hornak, C. de los Santos, A.P. Grollman, C. Simmerling, Computational analysis of the mode of binding of 8-oxoguanine to formamidopyrimidine–DNA glycosylase, Biochemistry 45 (2006) 10886–10894, https://doi.org/10.1021/bi060380m.
[59] K. Song, C. Kelso, C. de los Santos, A.P. Grollman, C. Simmerling, Molecular simulations reveal a common binding mode for glycosylase binding of oxidatively damaged DNA lesions, J. Am. Chem. Soc. 129 (2007) 14536–14537, https://doi.org/10.1021/ja075128w.
[60] C. Bergonzo, A.J. Campbell, C. de los Santos, A.P. Grollman, C. Simmerling, Energetic preference of 8-oxoG eversion pathways in a DNA glycosylase, J. Am. Chem. Soc. 133 (2011) 14504–14506, https://doi.org/10.1021/ja205142d.
[61] H. Li, A.V. Endutkin, C. Bergonzo, A.J. Campbell, C. de los Santos, A. Grollman, D.O. Zharkov, C. Simmerling, A dynamic checkpoint in oxidative lesion discrimination by formamidopyrimidine–DNA glycosylase, Nucleic Acids Res. 44 (2016) 683–694, https://doi.org/10.1093/nar/gkv1092.
[62] A. Prakash, B.L. Carroll, J.B. Sweasy, S.S. Wallace, S. Doublié, Genome and cancer single nucleotide polymorphisms of the human NEIL1 DNA glycosylase: activity, structure, and the effect of editing, DNA Repair 14 (2014) 17–26, https://doi.org/10.1016/j.dnarep.2013.12.003.
[63] J.T. Vivian, P.R. Callis, Mechanisms of tryptophan fluorescence shifts in proteins, Biophys. J. 80 (2001) 2093–2109, https://doi.org/10.1016/S0006-3495(01)76183-8.
[64] K.V. Simon-Lukasik, A.V. Persikov, B. Brodsky, J.A.M. Ramshaw, W.R. Laws, J.B.A. Ross, R.D. Ludescher, Fluorescence determination of tryptophan side-chain accessibility and dynamics in triple-helical collagen-like peptides, Biophys. J. 84 (2003) 501–508, https://doi.org/10.1016/S0006-3495(03)74869-3.
[65] D.L. Bunker, B. Garrett, T. Kliendienst, G.S. Long III, Discrete simulation methods in combustion kinetics, Combust. Flame 23 (1974) 373–379, https://doi.org/10.1016/0010-2180(74)90120-5.
[66] D.T. Gillespie, A general method for numerically simulating the stochastic time evolution of coupled chemical reactions, J. Comput. Phys. 22 (1976) 403–434, https://doi.org/10.1016/0021-9991(76)90041-3.
[67] E.I. Zaika, R.A. Perlow, E. Matz, S. Broyde, R. Gilboa, A.P. Grollman, D.O. Zharkov, Substrate discrimination by formamidopyrimidine–DNA glycosylase: a mutational analysis, J. Biol. Chem. 279 (2004) 4849–4861, https://doi.org/10.1074/jbc.M310262200.

[68] C. Cao, Y.L. Jiang, J.T. Stivers, F. Song, Dynamic opening of DNA during the enzymatic search for a damaged base, Nat. Struct. Mol. Biol. 11 (2004) 1230–1236, https://doi.org/10.1038/nsmb864.

[69] L.Y. Kanazhevskaya, V.V. Koval, D.O. Zharkov, P.R. Strauss, O.S. Fedorova, Conformational transitions in human AP endonuclease 1 and its active site mutant during abasic site repair, Biochemistry 49 (2010) 6451–6461, https://doi.org/10.1021/bi100769k.

[70] I.R. Grin, S.N. Khodyreva, G.A. Nevinsky, D.O. Zharkov, Deoxyribophosphate lyase activity of mammalian endonuclease VIII-like proteins, FEBS Lett. 580 (2006) 4916–4922, https://doi.org/10.1016/j.febslet.2006.08.011.

[71] P. Kuzmic, Program DYNAFIT for the analysis of enzyme kinetic data: application to HIV proteinase, Anal. Biochem. 237 (1996) 260–273, https://doi.org/10.1006/abio.1996.0238.

[72] R. Fraczkiewicz, W. Braun, Exact and efficient analytical calculation of the accessible surface areas and their gradients for macromolecules, J. Comput. Chem. 19 (1998) 319–333, https://doi.org/10.1002/(SICI)1096-987X(199802)19:3<319::AID-JCC6>3.0.CO;2-W.

[73] F. Sievers, A. Wilm, D. Dineen, T.J. Gibson, K. Karplus, W. Li, R. Lopez, H. McWilliam, M. Remmert, J. Söding, J.D. Thompson, D.G. Higgins, Fast, scalable generation of high-quality protein multiple sequence alignments using Clustal Omega, Mol. Syst. Biol. 7 (2011) 539, https://doi.org/10.1038/msb.2011.75.